Available online at www.sciencedirect.com
SCIENCE DIRECT®
Journal of Magnetic Resonance 168 (2004) 220–227
JMR Journal of Magnetic Resonance
www.elsevier.com/locate/jmr

Fast EPR imaging at 300 MHz using spinning magnetic field gradients

Yuanmu Deng, Guanglong He, Sergy Petryakov, Periannan Kuppusamy, and Jay L. Zweier*

Center for Biomedical EPR Spectroscopy and Imaging, The Davis Heart and Lung Research Institute, and The Division of Cardiovascular Medicine, The Department of Internal Medicine, The Ohio State University College of Medicine, Columbus, OH 43210, USA

Received 7 January 2004; revised 9 February 2004
Available online 1 April 2004

Abstract

Electron paramagnetic resonance imaging (EPRI) technology has rapidly progressed in the last decade enabling many important applications in the fields of biology and medicine. At frequencies of 300–1200 MHz a range of in vivo applications have been performed. However, the requisite imaging time duration to acquire a given number of projections, limits the use of this technique in many in vivo applications where relatively rapid kinetics occur. Therefore, there has been a great need to develop approaches to accelerate EPRI data acquisition. We report the development of a fast low-frequency EPRI technique using spinning magnetic field gradients (SMFG). Utilizing a 300 MHz CW (continuous wave) EPRI system, SMFG enabled over 10-fold accelerated acquisition of image projections. 2D images with over 200 projections could be acquired in less than 3 s and with 20 s acquisitions good image quality was obtained on large aqueous free radical samples. This technique should be particularly useful for in vivo studies of free radicals and their metabolism.

Keywords: Fast EPR imaging; Fast magnetic resonance imaging; Free radicals; Image reconstruction; Spinning magnetic field gradient; Trityl

1. Introduction

As a unique technique capable of detecting and imaging free radicals, electron paramagnetic resonance imaging (EPRI) has achieved remarkable progress in a variety of applications in the fields of biology and medicine [1–10]. Despite its unique capability and specificity for free radical imaging, EPRI still has some technical limitations. Among these technical limitations is the relatively long time required for image acquisition. For example, it typically takes several minutes for a conventional EPR imaging system to acquire a 2D image and tens of minutes for a 3D image [11]. The long imaging time prevents the use of this technique in many biological applications where the free radicals have a short lifetime or a fast metabolic clearance [12]. Therefore, there is a great need to develop fast EPRI techniques.

Technically, EPRI techniques can be divided into two different types: time-domain and continuous wave (CW) EPRI techniques. The time-domain (also known as pulsed) EPRI technique, is much faster in imaging speed than the CW EPRI technique. For example, it has been demonstrated that with proper spin probes, a 3D EPR image can be acquired within several minutes using this technique [13]. However, due to the dead time of the EPR resonators and the relaxation limitations, the time-domain EPRI technique greatly restricts the use of spin probes. Basically only narrow-line spin probes can be used [13]. Because of this, the CW EPRI technique still dominates current applications. Its ability to image a broad variety of spin probes without restrictions based on linewidth is a major advantage as well as its superior sensitivity. In spite of these advantages over the time-domain EPRI technique, the CW EPRI technique requires more time

* Corresponding author.
E-mail address: zweier-1@medctr.osu.edu (J.L. Zweier).

1090-7807/$ - see front matter © 2004 Elsevier Inc. All rights reserved.
doi:10.1016/j.jmr.2004.02.012

for projection acquisition due to the nature of the field-sweep. To reduce the long imaging time, a fast field-scanning EPRI apparatus was constructed by Demsar et al. [14] for detection of diffusion and distribution of oxygen. In 1996, Oikawa et al. [15] developed a fast EPRI system based on fast field-scanning, which was able to acquire a 3D image within 1.5 min (81 projections were acquired). Recently, Ohno and Watanabe [16] proposed an alternative fast EPR imaging approach based on the spinning magnetic field gradients (SMFG) technique and feasibility studies on two small crystals of lithium phthalocyanine (LiPc) were performed at *X*-band. In comparison with the fast field-sweep technique that requires a specialized field-scanning coil and the related compensation algorithm, this technique has the advantage of relatively low hardware requirement. In principle, no modifications need to be made to the existing magnet and gradients of a conventional EPRI system assuming that the gradients have a low inductance and sufficiently rapid response time.

In this work, we report the development of a low-frequency high-speed EPRI system using SMFG. To apply SMFG to low-frequency EPRI, there are a number of technical challenges. First, the fast EPR imaging technique relies on the sensitivity of the imaging system that is directly proportional to the EPR working frequency. Thus, the same fast imaging technique feasible at high frequency does not necessarily work well at low frequency due to the lower sensitivity. Second, in low-frequency EPRI that is uniquely suited for the imaging of large living samples, the image quality is subject to the field inhomogeneity and the gradient nonlinearity that occur over the large object to be imaged and the requisite large field of view (FOV). In this case, the introduction of a spinning magnetic field gradient may induce additional image distortion such as geometric deformation that becomes more noticeable over the large FOV. Thus, special efforts are needed to investigate the hardware-related compensation and to optimize the imaging parameters. Additionally, a number of critical questions have not been previously addressed. For example, in the SMFG technique, the imaging time is proportional to the number of field sweep steps. Therefore, it is very important to investigate the optimal number of steps of field sweep, for a given set of imaging parameters, so as to shorten the imaging time without sacrificing image quality.

In this study, we report both hardware and software approaches and development to implement the SMFG technique to achieve fast EPR imaging in low-frequency applications. We evaluate the technique compared to the standard stepped gradient approach and show that marked acceleration of image acquisition can be realized.

2. Theory

2.1. Fast EPR imaging by spinning magnetic field gradients

Mathematically, the data acquisition process in a 2D conventional CW EPRI experiment are in essence equivalent to filling the following projection matrix **P**.

$$\mathbf{P}=\begin{bmatrix} p(r_1,\theta_1) & p(r_1,\theta_2) & \cdots & p(r_1,\theta_{N-1}) & p(r_1,\theta_N) \\ p(r_2,\theta_1) & p(r_2,\theta_2) & \cdots & p(r_2,\theta_{N-1}) & p(r_2,\theta_N) \\ \vdots & \vdots & \ddots & \vdots & \vdots \\ p(r_{M-1},\theta_1) & p(r_{M-1},\theta_2) & \cdots & p(r_{M-1},\theta_{N-1}) & p(r_{M-1},\theta_N) \\ p(r_M,\theta_1) & p(r_M,\theta_2) & \cdots & p(r_M,\theta_{N-1}) & p(r_M,\theta_N) \end{bmatrix}, \tag{1}$$

where

$$\begin{aligned} p(r,\theta) &= \int_L f(x,y)\,\mathrm{d}u \\ &= \int_{-\infty}^{\infty}\int f(x,y)\delta(x\cos\theta + y\sin\theta - r)\,\mathrm{d}x\,\mathrm{d}y \\ &\quad -\infty < r < \infty, \quad 0 \leqslant \theta < \pi. \end{aligned} \tag{2}$$

Refer to Fig. 1. Since a projection in CW EPRI is acquired by fixing θ (fixing magnetic field gradient) and varying r (sweep field), the above matrix is actually filled column by column. The imaging time is, therefore, determined by the speed of field-scanning, provided reasonable signal-to-noise ratio can be achieved. In the SMFG technique, however, a pseudo projection is acquired by fixing r and varying θ continuously (spinning

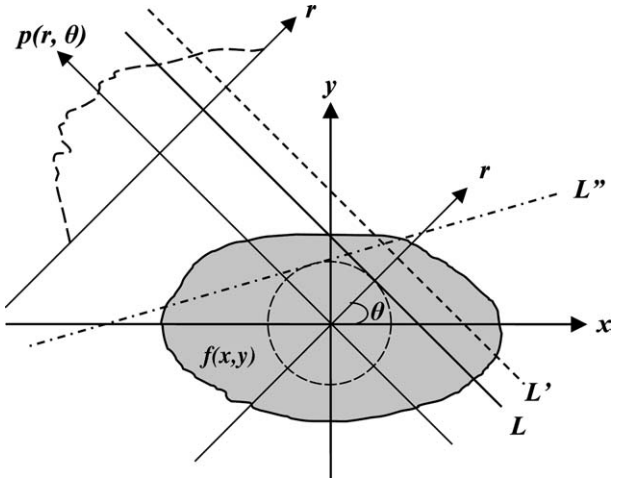

Fig. 1. Illustration of acquisition of projections in EPRI. Each element in the projection matrix **P**, i.e., $p(r,\theta)$, is a linear integration of the object $f(x,y)$ along the line $\boldsymbol{L}$. For a regular projection, $\boldsymbol{L}$ is a set of lines perpendicular to r (see dashed line $\boldsymbol{L}'$) while for a pseudo projection, $\boldsymbol{L}$ is a set of tangents to the dashed circle (see dash-dotted line $\boldsymbol{L}''$). Deconvolution process is needed in EPRI due to the large linewidth of EPR signals.

gradient). The matrix is filled row by row. In this case, the imaging time is determined by the spinning frequency of the gradient vector, which can readily reach to as high as tens of Hertz without special hardware modification to the existing gradient coils that were operated in non-resonant mode. In principle, the SMFG technique has the fundamental advantage compared to standard stepped gradient acquisition, in that it enables acquisition of an unlimited number of projections in one field sweep of the main magnet rather than requiring a field sweep for each projection.

2.2. Estimation of the minimal number of field-sweep steps

In the SMFG technique, the imaging time is proportional to the number of steps of field sweep, denoted as N_{step} hereafter. The more steps of field sweep, the higher the spatial resolution of projections but the longer the imaging time if other imaging parameters such as gradient strength are kept the same. Considering the acquisition of the zero-gradient projection in EPRI, the minimal number of steps of field sweep is determined essentially by the band width of the zero-gradient projection according to Shannon's sampling theorem. In our work, N_{step} is determined experimentally according to the sampling error [17] of the simulated zero-gradient projection (see Figs. 2A and B) as follows. Given the imaging parameters, a noise-free zero-gradient projection is simulated. Then the cutoff frequency f_c is determined by

$$|F(f)| \leqslant \beta \cdot |F(f)|_{\max} \text{ for } f \geqslant f_c. \quad (3)$$

Here $|F(f)|$ is the Fourier amplitude spectrum of the zero-gradient projection and $|F(f)|_{\max}$ is the maximum value of $|F(f)|$ and β is a predefined threshold. Denoting the scanning width as α, the N_{step} is determined by

$$N_{\text{step}} = \text{round}(2\alpha f_c). \quad (4)$$

In the simulation, the first derivative of Lorentzian lineshape function is used. The linewidth is 0.05 mT and the field scan width is 1.2 mT (see Fig. 2 for more description). From the sampling error curve, one can determine that the minimal number of steps for field sweep is slightly larger than 64 but less than 128. Therefore, we used either 64 or 128 steps for field sweep in the fast EPRI experiments.

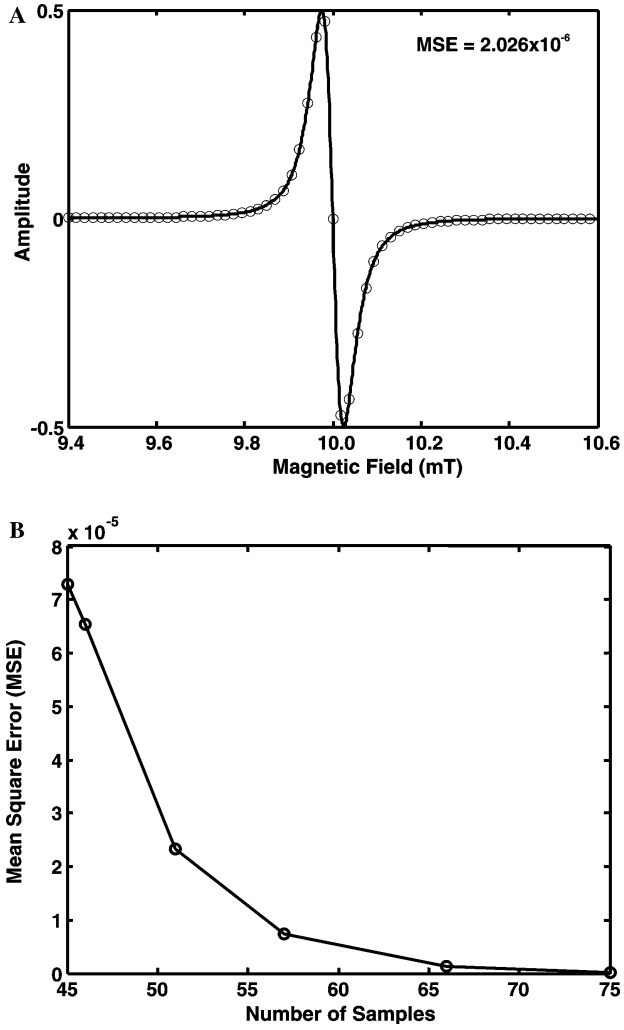

Fig. 2. Determination of the optimal number of steps of field sweep. (A) A simulated zero-gradient projection and the sampling results. The first derivative of Lorentzian lineshape is used with linewidth = 0.05 mT and scan width = 1.2 mT. 64 samples are sampled. The mean square error (MSE) between the original signal and the reconstruction result using 64 sampling points is 2.026×10^{-6}. (B) Sampling error varies with the number of steps of field sweep. The number of steps of field sweep was calculated using Eqs. (3) and (4), with $\beta = 0.09$, 0.07, 0.05, 0.03, 0.01, and 0.005, respectively.

3. Experimental

3.1. Hardware implementation

A schematic diagram illustrating the hardware implementation used for the SMFG fast EPR imaging is shown in Fig. 3. A solenoid electromagnet design with field homogeneity of about 3 ppm over a 10 cm DSV (diameter of spherical volume) is used, as was originally designed for use in nuclear magnetic resonance imaging [18]. The gradient system used (BFG-U-140-25, Resonance Research, Billerica, MA) offers a gradient linearity better than 1% over an 80 mm DSV. A transverse one-loop and two-bridged-gap resonator with inner modulation coils was used for the experiments shown. For this resonator and modulation coil assembly the maximum size sample that can be imaged is 40 mm in diameter and 80 mm in length. For a lossy sample simulating a biological object the size of a mouse consisting of a bottle containing 26 cc 0.5 mM TAM in 0.45% saline solution, a signal-to-noise ratio of 1000 was obtained for a 10 s acquisition or 2000 for a 40 s acquisition

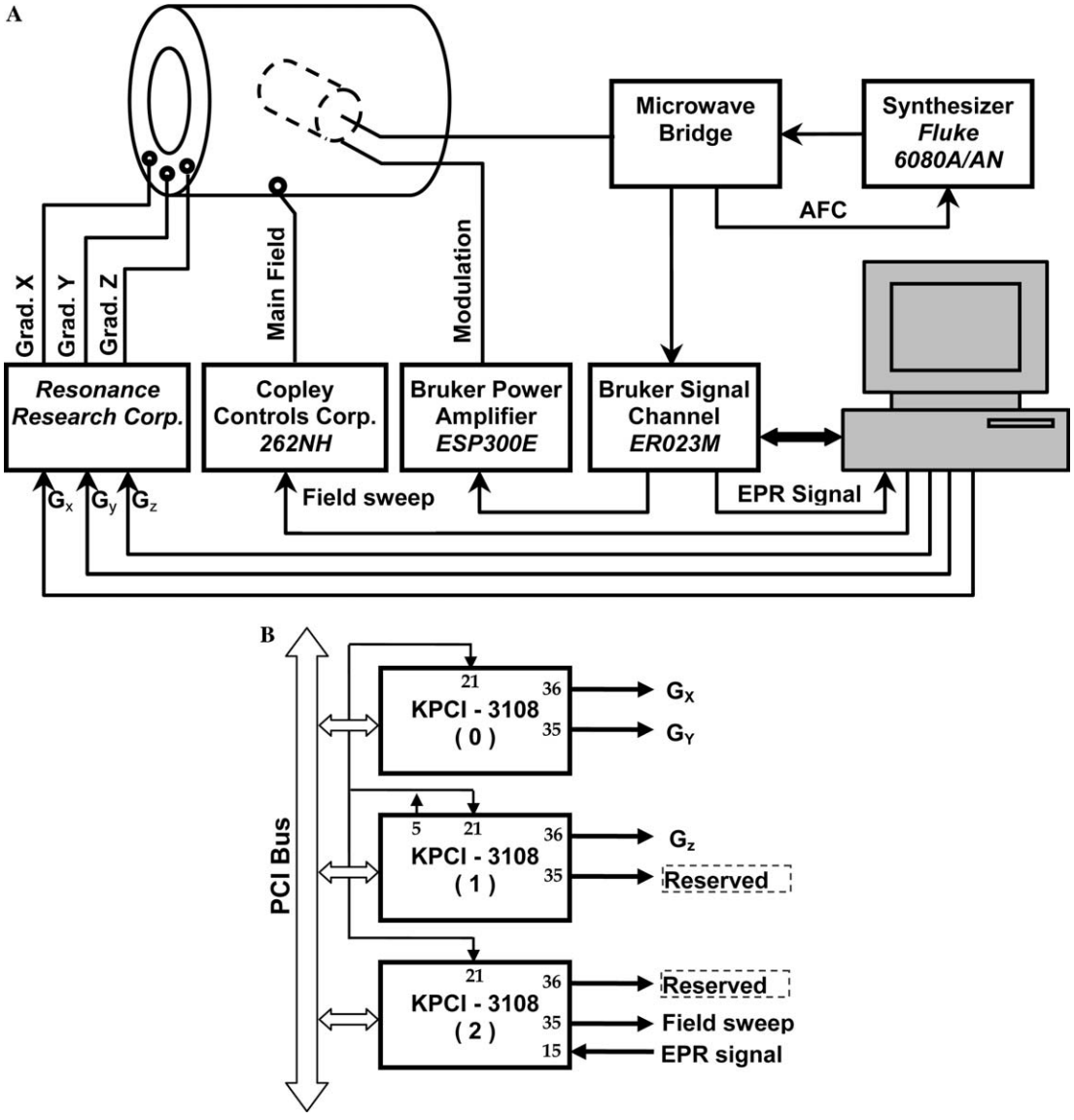

Fig. 3. Hardware implementation used for the SMFG fast EPR imaging. (A) Schematic diagram of the fast EPR imaging system. A solenoid electromagnet with a field homogeneity of about 3 ppm over a 10 cm DSV is used. The linearity of the gradient system (BFG-U-140-25, Resonance Research, Billerica, MA) is better than 1% over a 80 mm DSV. A transverse one-loop and two-bridged-gap resonator with inner modulation coils is used in the experiments, allowing a maximum size sample of 40 mm in diameter and 80 mm in length. (B) Diagram of generation of the field sweep signal and gradient waveforms using KPCI-3108 boards. The analog EPR signal is also sampled through the pin 15 of board 2. Pin 5 of board 1 outputs a square waveform that is used as an external clock by all three KPCI-3108 boards (through pin 21).

suggesting that 0.4×10^{16} spins could be detected in a relatively large lossy sample or a concentration of 0.25 μM TAM with an acquisition of less than 1 min. The specific details of this imaging system design are to be reported separately.

In our 300 MHz EPRI system, a personal computer (PC) equipped with one PCI-488 board (Capital Equipment Corporation, MA) and three KPCI-3108 boards (Keithley Instruments, OH) is used to control the data acquisition process and image reconstruction. As in our other EPR imaging systems [19,20], the Bruker signal channel is interfaced with the computer through a PCI-488 GPIB card. The KPCI-3108 boards are high-performance data acquisition boards capable of digital-to-analog (D/A) and/or analog-to-digital (A/D) conversion paced by either internal or external clock. They are used to output the field sweep signal and the gradient waveforms. Since each KPCI-3108 board has only two D/A outputs, we use three boards to obtain up to 6 analog outputs. For synchronization purpose, all the three boards are programmed to work in the external clock mode. The external clock signal is generated through the internal timer 1 and 2 (cascaded) of the board 1 (see Fig. 3). In this way, the three KPCI-3108 boards are synchronized. During the experiment, the Analog Input subsystem (AI) of Board 2 is also

activated to digitize the EPR signal coming from the analog output of the Bruker signal channel. The pacing frequency for D/A and A/D conversion is 10 kHz (up to 100 kHz) in our experiments.

Before starting an imaging experiment, the field sweep signal and the magnetic field gradient waveforms are calculated according to the imaging parameters, and stored in a chain of buffers that are accessible by the KPCI-3108 boards. During the experiment, the stored sweep field signal and the gradient waveforms are output to drive the main magnetic field power amplification and the gradient power amplification, respectively. In the meantime, the EPR signal (analog output from the Bruker signal channel) is sampled at the 10 kHz pacing frequency and stored in the computer for post-processing.

3.2. Amplitude compensation for magnetic field gradient

In the SMFG technique, the gradient coils are fed with AC current, not DC current as in a normal system. As a result, the gradient coils become inductive loads. In this case, the complex impedance (not the pure resistance) should be taken into account to compensate the gradient strength. We used the following equation to calculate the compensation coefficients for X, Y, and Z gradient coils.

$$C_i = \sqrt{1 + K_i\left(\frac{2\pi f_s L_i}{R_i}\right)^2} \quad i = x, y, z, \tag{5}$$

where f_s is the spinning frequency of the magnetic field gradient, L_i and R_i ($i = x, y, z$) are the measured inductance and resistance of the gradient coils and K_i is an experimentally adjustable parameter. In the 300 MHz imaging system, the inductance and resistance for the X, Y, and Z gradient coils were measured as 1.32 mH, 1.55 mH, 0.76 mH and 0.143, 0.166, and 0.266 Ω, respectively, while K_x, K_y, and K_z were experimentally set as 0.5, 0.4, and 1.0, respectively. From Eq. (5), it can be easily calculated that when $f_s = 24$ Hz a voltage increase of 9% ($C_z = 1.09$) is required for Z gradient coil to generate the same gradient strength as generated in the stepped-gradient experiments.

3.3. Data processing and image reconstruction

After data acquisition, the pseudo projections are smoothed and re-ordered to get the normal mode projections. The number of projections after data re-ordering equals the length of a pseudo projection, i.e., the sampling frequency (10 kHz) divided by the spinning frequency f_s. To reduce the time for data post-processing and image reconstruction, we down-sample each pseudo projection approximately by 2 but keep the projection number odd [16]. As in conventional EPR imaging experiments, both the zero-gradient projection and normal projections are acquired. Then, the automatic deconvolution algorithm [21] is used to deconvolve all projections before the filtered back-projection algorithm is performed for image reconstruction.

4. Results

Based on a 300 MHz conventional EPRI system, which we have recently built, we implemented fast 2D EPR imaging using SMFG, and tested it by imaging phantom objects. For comparison, we conducted both regular and fast EPR imaging experiments on each phantom.

In the regular imaging experiments using stepped gradients, the main magnetic field is swept continuously. A fixed length of 1024 points is acquired for each projection. The total image acquisition time is determined by the product of scan time with the number of projections. However, with the existing solenoidal magnet and the current regulated magnetic field control technique, the shortest scan time that could be used is 2.6 s. This limitation is primarily due to the time constant of the magnet and EPR signals are distorted with scan times less than 2.6 s. In the fast imaging experiments, the imaging time was controlled by the number of steps of field sweep and/or the spinning frequency, but not by the number of projections as in the stepped gradient acquisitions. As can be seen later, the time constant (TC) in SMFG fast imaging experiments is much less than that in regular stepped gradient imaging experiments.

4.1. Imaging of a strong non-lossy phantom

A phantom was constructed consisting of 7 tubes (id =3 mm) filled with DPPH (2,2-diphenyl-1-picrylhydrazyl) powder. Each tube was approximately 40 mm in length and separated from the others by at least 7.5 mm (central distance), as shown in Figs. 4A and B. In both regular and fast imaging experiments, the scan width (SW) = 4 mT, FOV = 70×70 mm^2 and modulation amplitude (MA) = 0.05 mT. The peak–peak linewidth of the DPPH spectrum measured at 300 MHz frequency was approximately 0.11 mT and the signal-to-noise ratio of the observed spectrum was >4000/1 for a 2.6 s acquisition. The image resolution is approximately 3.3 mm [22] and can be enhanced by a factor of 2–3 after deconvolution [23]. A regular image acquired using stepped gradients (gradient magnitude 57 mT/m) is shown in Fig. 4C. A total of 32 projections were acquired and the scan time of each projection was 2.6 s. Therefore, the total imaging time was 84 s. The time constant (TC) was 10 ms in the experiment. Fig. 4D shows the imaging result of the same phantom using the comparable SMFG technique. The number of steps of field sweep was 64 and the spinning frequency was

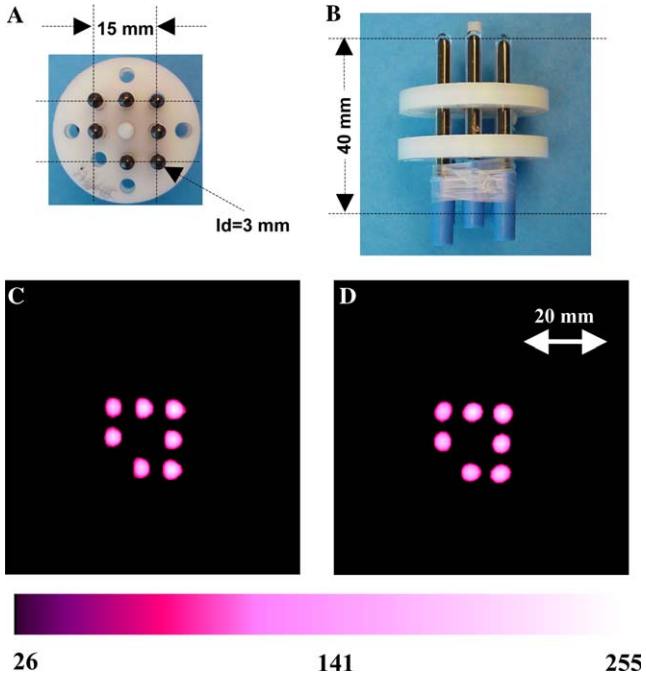

Fig. 4. Imaging of a strong non-lossy phantom. A phantom consisting of 7 tubes (id = 3 mm) filled with DPPH powder was used. Images A and B are the pictures of the phantom. Image C was acquired using stepped gradients while image D was acquired using the SMFG fast imaging technique. Parameters used in regular imaging experiment were: number of projections = 32; scan time = 2.6 s; time constant = 10 ms. Total imaging time was 84 s. Parameters for fast imaging experiment were: spinning frequency = 24 Hz; number of field sweep steps = 64; time constant = 0.64 ms. In both regular and fast imaging experiments, scan width = 4 mT; FOV = $70 \times 70\,mm^2$ and modulation amplitude = 0.05 mT. A total of 203 projections were acquired and the imaging time was 2.6 s.

24 Hz. The imaging time was therefore 2.6 s within which 203 projections were acquired. The time constant was fixed to 0.64 ms in the experiment. The signal-to-noise ratio, defined as the ratio of the mean of the pixels with an intensity higher than a predefined threshold to that of other non-signal pixels in an image, was measured for images 4C and D and was 32 and 149, respectively. The threshold was defined as 10% of the maximum intensity of the image after normalization in our experiments. Thus, we demonstrated that for a strong near noiseless sample such as this DPPH phantom about a 30-fold acceleration of image data collection was achieved.

4.2. Imaging of a large aqueous radical phantom

A large lossy aqueous phantom was constructed using a tapered cap bottle of 26 ml volume containing 0.5 mM TAM (triarylmethyl radical, OXO63, Nycomed Innovations, Malmö, Sweden) [24] in 0.45% saline solution. Both regular and fast imaging experiments used the following parameters: SW = 1.2 mT, FOV = $80 \times 80\,mm^2$

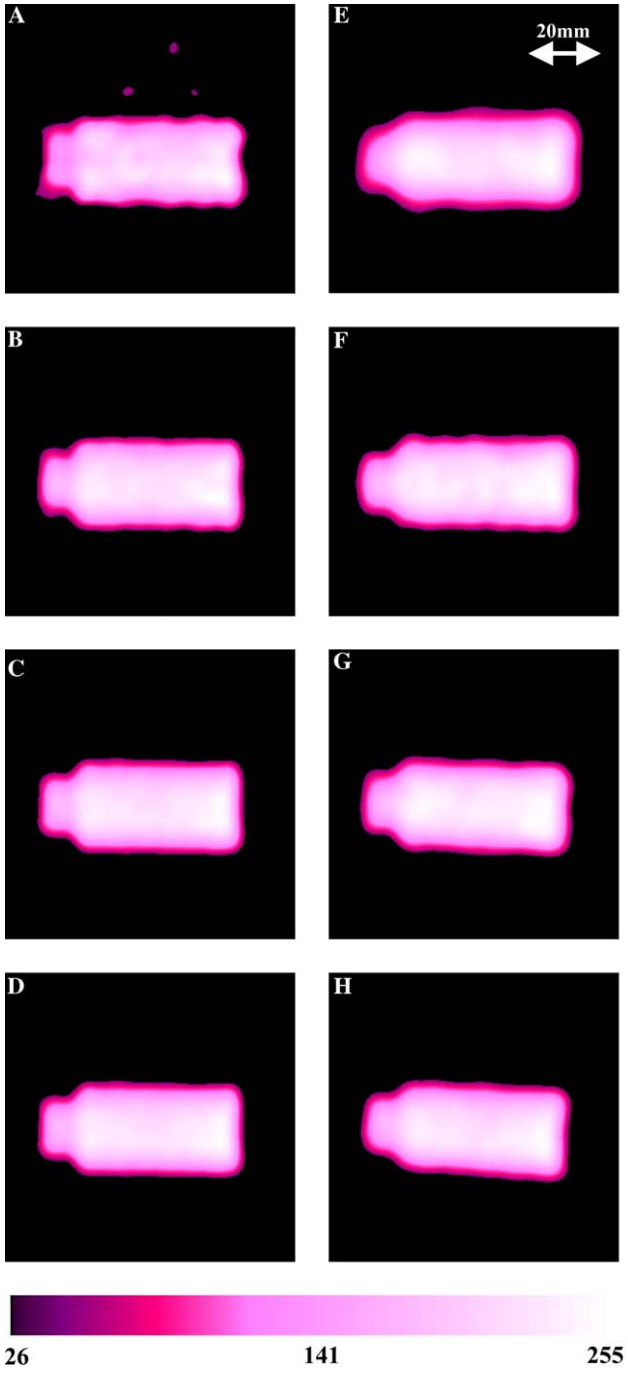

Fig. 5. Imaging of a large aqueous radical phantom. A lossy aqueous phantom was constructed using a bottle with tapered cap of 26 ml volume containing 0.5 mM TAM in 0.45% saline solution. Images A–D were acquired using conventional technique (field-sweep) with the following parameters (from A to D order): scan time = 2.6, 2.6, 2.6, and 10 s; time constant = 10, 10, 10, and 40 ms; number of projections = 8, 16, 32, and 32; imaging time = 21, 42, 84, and 320 s; Images E–H were acquired using fast imaging technique with the following parameters: spinning frequency = 12, 12, 6, and 3 Hz; number of steps = 64, 128, 128, and 128; number of projections = 409, 409, 819, and 1637; imaging time = 5, 11, 21, and 42 s. For all the images, modulation amplitude = 0.05 mT; scan width = 1.2 mT; FOV = $80 \times 80\,mm^2$. The signal-to-noise ratio for images A–H is 133, 300, 334, 366, 114, 291, 265, and 308, respectively.

and MA = 0.05 mT. The peak–peak linewidth of the TAM spectrum measured at 300 MHz frequency was approximately 0.05 mT (over-modulated) and the signal-to-noise ratio of the observed spectrum was about 400/1 for a 2.6 s acquisition. The image resolution is approximately 5.8 mm without deconvolution [22] and the resolution enhancement by deconvolution can be about a factor of 2 [23]. Regular images acquired using stepped gradients (gradient magnitude 15 mT/m) are shown in Figs. 5A–D. The imaging time for Figs. 5A–C with 8, 16, or 32 projections (scan time = 2.6 s) was 21, 42, or 84 s, respectively. To further optimize the projection signal-to-noise ratio an additional image was acquired over 320 s with 32 projections (scan time-= 10 s), Fig. 5D. The time constant was chosen according to the scan time with a value of 10 or 40 ms. The images acquired using the SMFG technique are shown in Figs. 5E–H, corresponding to the steps of field sweep of 64, 128, 128 or 128 and spinning frequencies of 12, 12, 6 or 3 Hz. The imaging time for Figs. 5E–H with 409, 409, 819 or 1639 projections was 5, 11, 21 and 42 s, respectively. As mentioned above, the time constant was 0.64 ms. The signal-to-noise ratio for images 5A–H is 133, 300, 334, 366, 114, 291, 265, and 308, respectively.

4.3. Summary of imaging results

In the DPPH phantom imaging experiment (Fig. 4), where signal-to-noise was not limiting, regular stepped gradient image data collection required over 84 s, while with the SMFG fast imaging technique, the image data was acquired over only 2.6 s. Since more than 200 projections were acquired, the quality of the fast image (Fig. 4D) is even better than that of the regular (stepped gradient) one acquired over 84 s. Thus, over 30-fold accelerated acquisition of image projections has been achieved.

The acceleration of projection acquisition has also been demonstrated in imaging experiments of the large lossy aqueous TAM-radical phantom. From Fig. 5, it can be easily seen that, in the regular imaging experiments, the image quality is poor when only 8 projections were used (Fig. 5A, 21 s). Doubling the projection number to 16 appeared to increase the image quality (Fig. 5B, 42 s). However, 32 projections (Fig. 5C, 84 s) may be needed in actual imaging applications to achieve desirable image quality. Certainly, the longest imaging time produced the best image quality (Fig. 5D, 320 s) but may not be feasible in some applications due to the fast metabolic clearance of the free radicals and/or the instability of the imaging system. Compared with the stepped gradient imaging technique, the SMFG fast EPRI technique is able to achieve a better tradeoff between the image quality and the image acquisition time. For example, within 5 s, we obtained a reasonable 2D EPR image (Fig. 5E), which looks better than the image acquired in 21 s using the regular technique (Fig. 5A). From a practical application point of view, 21 s may be needed (Fig. 5G) to obtain good image quality using the fast imaging technique under the conditions used in the measurements. From Fig. 5, it is clear that, with a slight loss of signal-to-noise ratio, the SMFG fast imaging technique was able to reduce the imaging time remarkably. A small 2.5° rotation of the image was seen between Figs. 5D and H due to the compensation error of Eq. (5). The results clearly demonstrate the feasibility of the SMFG technique for fast EPR imaging at low frequency.

5. Discussion

In conventional EPRI utilizing stepped gradient acquisition, the imaging time can be reduced by either acquiring a smaller number of projections or by reducing the field sweep time, or both. Obviously, there is a tradeoff between the spatial resolution and/or the signal-to-noise ratio of the image and the temporal resolution. However, due to the intrinsic bandwidth of the objects to be imaged and the hardware response time, the gain in temporal resolution is very limited. For example, with the 300 MHz imaging system, the shortest imaging time, even with only 8 projections, cannot be less than 20 s (see Fig. 5A). The SMFG fast imaging technique, on the other hand, has the great advantage of enabling much further reduction of the imaging time. With the SMFG technique the image speed can be reduced to the fundamental limit imposed by the signal-to-noise ratio of the measurements, assuming that the gradients have a low inductance and sufficiently rapid response time. For example, in the TAM-radical imaging experiments, the total number of spins was 0.78×10^{19} and the signal-to-noise ratio of the projection data was measured within the range 4–10. Under this condition, 20 s were required to acquire good quality 2D images using the SMFG fast imaging technique. However, if the number of spins is doubled, then only 5 s will be required to obtain a same quality image using the same fast imaging technique. Similar fast imaging techniques by rotating gradients have been well established in other imaging modalities such as spiral echo planar imaging (EPI) [25] and spiral computerized tomography (CT) [26,27]. Therefore, it is very intuitive to develop fast EPRI systems using SMFG, in order to reduce the imaging time.

Ohno and Watanabe [16] were the first to demonstrate the feasibility of utilizing the spinning gradient technique for EPR image acquisition. In their measurements at *X*-band they used 65 projections acquired at a spinning frequency of 20 Hz. To achieve comparable signal-to-noise ratio to their standard stepped gradient acquisition, they had to average 16 spinning gradient cycles. Our experiments evaluated the ability to implement this approach at 300 MHz on larger lossy

samples. We also evaluated the advantages of this technique in accelerating image acquisition and improving image quality. In our applications, the number of projections acquired was in the range from 203 to 1637. This is very critical in fast EPRI since the number of steps of field sweep is already reduced dramatically (typically reduced from 1024 to 128, even 64), therefore, the number of projections should be increased accordingly in order to achieve comparable spatial resolution. Otherwise, the image distortion due to insufficient projections will dominate the image quality in low-frequency EPRI because of the large FOV. The spinning frequency in our experiments varied from 3 to 24 Hz. Since we did not use signal averaging to increase signal-to-noise ratio, the overall imaging time in our experiments is much less than that in the earlier report [16]. There was no need for us to use higher spinning frequency with signal averages.

6. Conclusion

We developed and implemented a spinning magnetic field gradient acquisition system for low field EPR imaging at 300 MHz. This system is capable of acquiring a 2D image with more than 200 projections within 2.6 s. Good image quality was obtained with acquisition times 4- to 30-fold times faster than the conventional stepped gradient approach. This fast imaging technique with low field EPRI instrumentation should be particularly useful for the in vivo and ex vivo imaging of free radicals.

Acknowledgments

This work was supported by NIH Grants RR 12190/EB00306, GM58582/EB00254, and EB00890. We thank Scott Yano and Eric Kesselring for technical assistance.

References

[1] J.L. Berliner, H. Fujii, Magnetic resonance imaging of biological specimens by electron paramagnetic resonance of nitroxide spin labels, Science 227 (1985) 517–519.
[2] J.L. Zweier, P. Kuppusamy, Electron paramagnetic resonance measurements of free radicals in the intact beating heart: a technique for detection and characterization of free radicals in whole biological tissues, Proc. Natl. Acad. Sci. USA 85 (1988) 5703–5707.
[3] G.R. Eaton, S.S. Eaton, K. Ohno, EPR Imaging and In Vivo EPR, CRC Press, Boca Raton, 1991.
[4] M. Ferrari, V. Quaresima, A. Sotgiu, Present status of electron paramagnetic resonance (EPR) spectroscopy/imaging for free radical detection, Pflugers Arch. 431 (1996) R267–R268.
[5] V. Quaresima, M. Ferrari, Current status of electron spin resonance (ESR) for in vivo detection of free radicals, Phys. Med. Biol. 43 (1998) 1937–1947.
[6] H.M. Swartz, T. Walczak, Developing in vivo EPR oximetry for clinical use, Adv. Exp. Med. Biol. 454 (1998) 243–252.
[7] G.R. Eaton, S.S. Eaton, ESR imaging, in: C.P. Poole, H.A. Farach (Eds.), Handbook of Electron Spin Resonance, AIP Press:Springer, New York, 1999, pp. 327–343.
[8] C.P. Poole, H.A. Farach, Handbook of Electron Spin Resonance, AIP Press:Springer, New York, 1999.
[9] J.L. Berliner (Ed.), Biological Magnetic Resonance, vol. 18, Kluwer Academic/Plenum Publishers, New York, 2003.
[10] H.M. Swartz, J.F. Dunn, Measurements of oxygen in tissues: overview and perspectives on methods, Adv. Exp. Med. Biol. 530 (2003) 1–12.
[11] P. Kuppusamy, M. Chzhan, J.L. Zweier, Development and optimization of three-dimensional spatial EPR imaging for biological organs and tissues, J. Magn. Reson. B 106 (1995) 122–130.
[12] P. Kuppusamy, H. Li, G. Ilangovan, A.J. Cardounel, J.L. Zweier, K. Yamada, M.C. Krishna, J.B. Mitchell, Noninvasive imaging of tumor redox status and its modification by tissue glutathione levels, Cancer Res. 62 (2002) 307–312.
[13] K. Yamada, R. Murugesan, N. Devasahayam, J.A. Cook, J.B. Mitchell, S. Subramanian, M.C. Krishna, Evaluation and comparison of pulsed and continuous wave radiofrequency electron paramagnetic resonance techniques for in vivo detection and imaging of free radicals, J. Magn. Reson. 154 (2002) 287–297.
[14] F. Demsar, T. Walczak, P.D. Morse II, G. Bacic, Z. Zolnai, H.M. Swartz, Detection of diffusion and distribution of oxygen by fast-scan EPR imaging, J. Magn. Reson. 76 (1988) 224–231.
[15] K. Oikawa, T. Ogata, H. Togashi, H. Yokoyama, H. Ohya-Nishiguchi, H. Kamada, A 3D- and 4D-ESR imaging system for small animals, Appl. Radiat. Isot. 47 (1996) 1605–1609.
[16] K. Ohno, M. Watanabe, Electron paramagnetic resonance imaging using magnetic-field-gradient spinning, J. Magn. Reson. 143 (2000) 274–279.
[17] V.K. Ingle, J.G. Proakis, Digital Signal Processing using MATLAB, Brooks/Cole, Pacific Grove, CA, 2000.
[18] D.I. Hoult, S. Goldstein, J. Caponiti, Electromagnet for nuclear resonance imaging, Rev. Sci. Instrum. 52 (1981).
[19] P. Kuppusamy, M. Chzhan, K. Vij, M. Shteynbuk, D.J. Lefer, E. Giannella, J.L. Zweier, Three-dimensional spectral-spatial EPR imaging of free radicals in the heart: a technique for imaging tissue metabolism and oxygenation, Proc. Natl. Acad. Sci. USA 91 (1994) 3388–3392.
[20] G. He, R.A. Shankar, M. Chzhan, A. Samouilov, P. Kuppusamy, J.L. Zweier, Noninvasive measurement of anatomic structure and intraluminal oxygenation in the gastrointestinal tract of living mice with spatial and spectral EPR imaging, Proc. Natl. Acad. Sci. USA 96 (1999) 4586–4591.
[21] Y. Deng, G. He, P. Kuppusamy, J.L. Zweier, Deconvolution algorithm based on automatic cutoff frequency selection for EPR imaging, Magn. Reson. Med. 50 (2003) 444–448.
[22] M.J.R. Hoch, U. Ewert, Resolution in EPR imaging, in: G.R. Eaton, S.S. Eaton, K. Ohno (Eds.), EPR Imaging and In Vivo EPR, CRC Press, Boca Raton, 1991, pp. 153–159.
[23] W.E. Blass, G.W. Halsey, Deconvolution of Absorption Spectra, Academic Press, New York, 1981.
[24] P. Kuppusamy, P. Wang, M. Chzhan, J.L. Zweier, High resolution electron paramagnetic resonance imaging of biological samples with a single line paramagnetic label, Magn. Reson. Med. 37 (1997) 479–483.
[25] E.M. Haacke, Magnetic Resonance Imaging: Physical Principles and Sequence Design, Wiley-Liss, New York, 1999.
[26] E.K. Fishman, R.B. Jeffrey, Spiral CT: Principles, Techniques, and Clinical Applications, Lippincott-Raven, Philadelphia, 1998.
[27] M.L. Bahner, W. Reith, I. Zuna, R. Engenhart-Cabillic, G. van Kaick, Spiral CT vs incremental CT: is spiral CT superior in imaging of the brain? Eur. Radiol. 8 (1998) 416–420.